Validity Assessment of Ductile Fracture Criteria in Cold Forming

M.A. Shabara, A.A. El-Domiaty, and A. Kandil

This paper describes the assessment of various empirical and semiempirical ductile fracture criteria to determine their ability to predict the occurrence of fracture in metalforming processes. The criteria assessed are reformulated such that each is expressed in terms of mostly nondimensional material-dependent quantities and constants. The constants in each criterion are determined using data from published experimental results on cold upsetting of aluminum and steel specimens. The limit strain or the forming limit corresponding to each criterion is then determined and compared with the experimental data. There is clearly good agreement between theory and experiment for several criteria, but the predictions of other criteria fall far from experimental results.

Keywords
ductile fracture, forming, fracture criteria, limit diagrams, metalforming

1. Introduction

THE LIMITING factor in many metalforming processes is the occurrence of ductile fracture, which is characterized by void initiation at second-phase particles and inclusions, strain-controlled growth, and finally coalescence of the growing voids. Many ductile fractures, such as edge cracking in rolling, chevron and internal cracking in extrusion, tears in sheet-metal forming, and laps and surface cracks in forging, have been identified in industrial metalforming operations. The ability to predict ductile failure leads to the reduction of failure in existing metalforming processes and allows for early modification of the production process by increasing workability of the material.

In the absence of a reliable quantitative model for estimating the ductility of a material undergoing large plastic flow in a metalforming or metalworking process, a number of phenomenological models of metal-processing ductility have been developed. However, no general theoretical means of predicting the occurrence of this type of failure has been advanced, and the successful avoidance of fracture has been largely a matter of empirical practice.

A review of ductile fracture criteria is given by Clift and Hartley (Ref 1), who classified published fracture criteria into two categories: "theoretical models of void coalescence and growth" and "empirical and semiempirical models." In addition to models of fracture, criteria have been developed from macroscopic concepts of fracture. Oyane et al. (Ref 2, 3) based their simple criterion on the assumption that fracture of the material occurs when a critical material-dependent volumetric strain is attained. The Oyane empirical criterion of ductility is successful to the extent that it identifies some of the important parameters that determine ductility in metalworking processes.

M.A. Shabara and **A.A. El-Domiaty,** Department of Mechanical & Industrial Engineering, Kuwait University, Kuwait; and **A. Kandil,** Department of Mechanical Design & Production, Port Said University, Port Said, Egypt.

A generalized plastic work criterion has been developed by Freudenthal (Ref 4), who postulated that a critical value of strain energy should be stored in the material in order for fracture to occur. Cockcroft and Latham (Ref 5) concluded from their experiments on mild steel tensile specimens that the integral of tensile plastic work per unit volume must reach a critical, material-dependent value for fracture to occur. This criterion is actually a special case of that of Freudenthal and has been developed on similar principles. Brozzo et al. (Ref 6) proposed an empirical modification to the Cockcroft and Latham criterion where the mean stress was taken into account to improve correlation with experimental results. Oh et al. (Ref 7, 8) introduced another modification to the Cockcroft and Latham fracture criterion by considering the ratio of maximum tensile stress to generalized stress as the major parameter controlling ductile fracture. Osakada and Mori (Ref 9) developed a criterion that includes an explicit dependence on generalized plastic strain.

With these forms of semiempirical equations, the material constants are determined by experiments on the appropriate material. On the other hand, the finite-element method (FEM) has been used to simulate and analyze deformation in a number of forming processes (Ref 1, 10-13). The FEM provides details of stresses, strains, strain rates, and temperatures throughout the formed material and their history throughout the process. The purpose of the present work is to assess the applicability of the empirical and semiempirical models of ductile fracture to predict the forming limit curve and compare it with experimental data available in the literature.

2. Analysis

2.1 *Compression Test as a Measure of Workability*

Workability, or the relative ease with which a metal can be formed plastically, is not a unique property of the material but depends on such process variables as strain, strain rate, temperature, friction, and the stress system imposed by the process. Workability can be expressed in terms of the ductility of the material as well as the stresses and strains imposed by the process.

Therefore, to describe workability a fracture criterion must be established that defines the limit of strain as a function of

strain rate and temperature. An experimental approach that uses this concept of workability is the forming limit diagram, which is determined by conducting compression (upsetting) experiments.

The upsetting of a small cylinder at room temperature is one of the most widely used workability tests. As a metallic cylinder is compressed in the presence of friction, it usually tends to barrel, and a biaxial stress state develops at the equator of the cylinder (Fig. 1). The stress state usually consists of a circumferential tensile stress and an axial compressive stress, although an axial tension stress may develop when barreling is severe. The surface strains measured at the onset of fracture for a wide range of test conditions enable construction of a fracture or forming limit diagram for the material. In the absence of friction, the tensile strain is equal to one-half of the compressive strain. Increasing the frictional constraint causes bulge severity to increase, which in turn increases the tensile strain and decreases the compressive strain. Beginning with the strain ratio of one-half for frictionless deformation, the strain-path slope increases with increasing friction. A wide range of strain paths (Fig. 2) can be produced at the free surfaces of cylindrical specimens, permitting evaluation of the fracture or forming limit of the material.

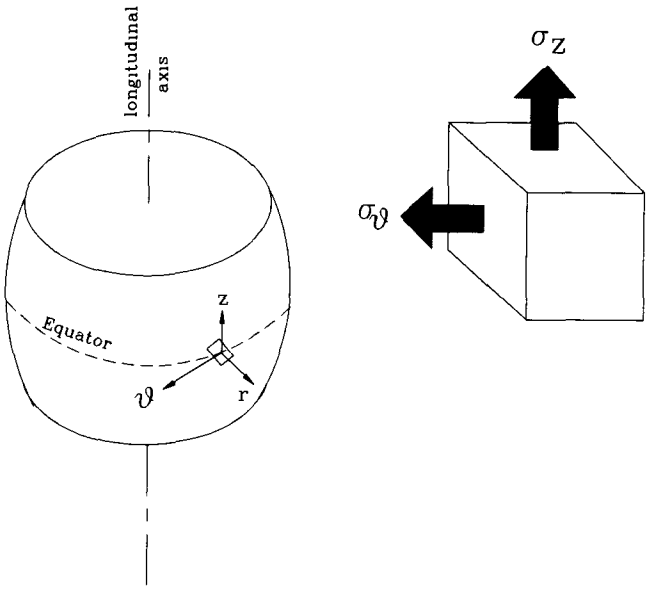

Fig. 1 Barreled compression specimen and the biaxial stress state on an element at the equatorial free surface

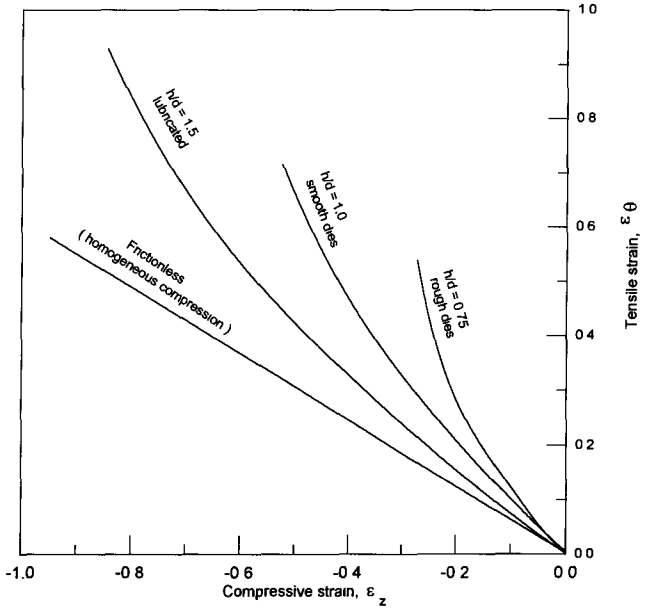

Fig. 2 Strain paths for compression specimens at various aspect ratios and friction conditions

2.2 *Stress-Strain Relations*

The components of stress and strain at the free surface of a compressed cylinder can be given as:

$$d\varepsilon_z = \frac{d\bar{\varepsilon}}{\bar{\sigma}}\left(\sigma_z - \frac{1}{2}\sigma_\theta\right) \quad \text{(Eq 1)}$$

$$d\varepsilon_r = \frac{-d\bar{\varepsilon}}{2\bar{\sigma}}(\sigma_z + \sigma_\theta)$$

$$d\varepsilon_\theta = \frac{d\bar{\varepsilon}}{\bar{\sigma}}\left(\sigma_\theta - \frac{1}{2}\sigma_z\right)$$

The effective strain increment is given by:

$$d\bar{\varepsilon} = \sqrt{\frac{2}{3}}\sqrt{(d\varepsilon_r^2 + d\varepsilon_\theta^2 + d\varepsilon_z^2)} \quad \text{(Eq 2)}$$

The mean or hydrostatic stress, σ_m, is given by:

$$\sigma_m = \frac{\sigma_r + \sigma_\theta + \sigma_z}{3} = \frac{\sigma_\theta + \sigma_z}{3}; \quad \text{(Eq a)}$$

$\sigma_r = 0$ at the surface of the cylinder.

From Eq 1, it is found that:

$$\frac{d\bar{\varepsilon}}{\bar{\sigma}} = \frac{d\varepsilon_\theta + d\varepsilon_z - d\varepsilon_r}{(\sigma_\theta + \sigma_z)} \quad \text{(Eq b)}$$

Table 1 Values of k and n for test mateirals at room temperature

Material	k, MPa	n
Commercially pure aluminum	180	0.20
Spheroidized 1% C steel	530	0.26
Low-carbon boron steel	723	0.31

For constant volume conditions, the summation of the strain increments is zero; that is:

$$d\varepsilon_r + d\varepsilon_\theta + d\varepsilon_z = 0 \qquad \text{(Eq c)}$$

By combining Eq a, b, and c, we get:

$$\frac{\sigma_m}{\bar{\sigma}} = -\frac{2}{3}\frac{d\varepsilon_r}{d\bar{\varepsilon}} \qquad \text{(Eq d)}$$

Then,

$$\frac{\sigma_m}{\bar{\sigma}} = \frac{1}{\sqrt{3}}\frac{\beta + 1}{\sqrt{\beta^2 + \beta + 1}} \qquad \text{(Eq 3)}$$

where β, the strain increment ratio, is the slope of the strain path, or:

$$\beta = \frac{d\varepsilon_\theta}{d\varepsilon_z} \qquad \text{(Eq e)}$$

Also from Eq 2, the effective strain increment is:

$$d\bar{\varepsilon} = \frac{2}{\sqrt{3}}\sqrt{\beta^2 + \beta + 1}\, d\varepsilon_z \qquad \text{(Eq 4)}$$

By integration, Eq 4 becomes:

$$\bar{\varepsilon} = \frac{2}{\sqrt{3}}\int_0^{\varepsilon_f}\sqrt{\beta^2 + \beta + 1}\, d\varepsilon_z \qquad \text{(Eq 5)}$$

The effective stress can also be expressed as a function of the strain increment ratio (β) and the tensile stress component (σ_θ) as follows:

$$\bar{\sigma} = \frac{\sqrt{3}\sqrt{\beta^2 + \beta + 1}}{(2\beta + 1)}\sigma_\theta \qquad \text{(Eq 6)}$$

From Eq 3, the mean stress can be expressed in the form:

$$\sigma_m = \frac{\bar{\sigma}}{\sqrt{3}}\frac{\beta + 1}{\sqrt{\beta^2 + \beta + 1}} = \frac{k\bar{\varepsilon}^n}{\sqrt{3}}\frac{\beta + 1}{\sqrt{\beta^2 + \beta + 1}} \qquad \text{(Eq 7)}$$

where k and n are material constants determined from the flow curve.

2.3 *Ductile Fracture Criteria*

The following sections examine six widely recognized fracture criteria developed by several authors to describe ductile fracture. Using the equations developed in the previous section, each criterion will be reformulated and presented, in a simple form, in terms of the strain increment ratio, β.

2.3.1 Oyane Fracture Criterion

Oyane et al. (Ref 2, 3) postulated that fracture occurs when a critical material-dependent volumetric strain is reached. The general form of the criterion is given as:

$$\bar{\varepsilon}_f = -\frac{1}{A}\int_0^{\bar{\varepsilon}_f}\frac{\sigma_m}{\bar{\sigma}}d\bar{\varepsilon} + C \qquad \text{(Eq 8)}$$

By substituting Eq 3 and 4 into Eq 8, the effective fracture strain, $\bar{\varepsilon}_f$, becomes:

$$\bar{\varepsilon}_f = \frac{-2}{3A}\int_0^{\varepsilon_{zf}}(\beta + 1)d\varepsilon_z + C \qquad \text{(Eq 9)}$$

where $\bar{\varepsilon}_f$ is given by Eq 5.

2.3.2 Freudenthal Fracture Criterion

Freudenthal (Ref 4) postulated that the critical parameter in the plastic deformation process is the strain energy to fracture. This is expressed as:

$$\int_0^{\bar{\varepsilon}_f}\bar{\sigma}\, d\bar{\varepsilon} = C_1 \qquad \text{(Eq 10)}$$

For many engineering materials, the relationship between $\bar{\sigma}$ and $\bar{\varepsilon}$ is given in the form of a power-law equation, $\bar{\sigma} = k\bar{\varepsilon}^n$, where k is the strength coefficient and n is the strain-hardening exponent; both are given in Table 1 for steel and aluminum alloys.

By substituting $\bar{\sigma} = k\bar{\varepsilon}^n$ into Eq 10 and integrating, the left-hand side of Eq 10 becomes:

$$\int_0^{\bar{\varepsilon}_f}\bar{\sigma}\, d\bar{\varepsilon} = \frac{k\bar{\varepsilon}_f^{n+1}}{n+1} \qquad \text{(Eq f)}$$

By substituting $\bar{\varepsilon}_f$ from Eq 5 into Eq f, the Freudenthal fracture criterion takes the form:

$$\frac{k\left(\frac{2}{\sqrt{3}}\int_0^{\varepsilon_{zf}}\sqrt{\beta^2 + \beta + 1}\, d\varepsilon_z\right)^{n+1}}{n+1} = C_1 \qquad \text{(Eq 11)}$$

2.3.3 Cockcroft and Latham Criterion

Cockcroft and Latham (Ref 5) used tensile test specimens of EN2A mild steel, which show a well-defined neck at fracture. They concluded that the integral of tensile plastic work per unit volume must reach a critical value for fracture to occur. This fracture criterion is expressed in terms of the maximum tensile stress, σ_θ, and takes the form:

$$\int_0^{\bar{\varepsilon}_f} \sigma_\theta \, d\bar{\varepsilon} = C_2 \qquad \text{(Eq 12)}$$

From Eq 7:

$$\sigma_\theta = \frac{2\beta + 1}{\sqrt{3}\sqrt{\beta^2 + \beta + 1}} \bar{\sigma}$$

Then, Eq 12 can be rewritten in the form:

$$\int_0^{\bar{\varepsilon}_f} \frac{2\beta + 1}{\sqrt{3}\sqrt{\beta^2 + \beta + 1}} \bar{\sigma} \, d\bar{\varepsilon} = C_2$$

Also,

$$\int_0^{\bar{\varepsilon}_f} \frac{2\beta + 1}{\sqrt{3}\sqrt{\beta^2 + \beta + 1}} k \, \bar{\varepsilon}^n \, d\bar{\varepsilon} = C_2$$

Then,

$$\frac{k}{\sqrt{3}} \int_0^{\varepsilon_{zf}} \frac{2\beta + 1}{\sqrt{3}\sqrt{\beta^2 + \beta + 1}} \bar{\varepsilon}^n \, d\varepsilon_z = C_2$$

$$\frac{2k}{3} \int_0^{\varepsilon_z f} (2\beta + 1) \left(\frac{2}{\sqrt{3}} \int_0^{\varepsilon_{zf}} \sqrt{\beta^2 + \beta + 1} \, d\varepsilon_z \right)^n d\varepsilon_z = C_2 \qquad \text{(Eq 13)}$$

2.3.4 Brozzo et al. Criterion

Brozzo et al. (Ref 6) proposed an empirical modification to the Cockcroft and Latham fracture criterion because it predicted generalized strains at fracture that were too low when compared with experimental results for sheet forming. This fracture criterion is expressed in terms of the maximum tensile stress and the mean stress and takes the form:

$$\int_0^{\bar{\varepsilon}_f} \frac{2\sigma_\theta}{3(\sigma_\theta - \sigma_m)} d\bar{\varepsilon} = C_3 \qquad \text{(Eq 14)}$$

By combining Eq 3 and 7, the ratio σ_m/σ_θ can be expressed as a function of the strain increment ratio, β, as follows:

$$\frac{\sigma_m}{\sigma_\theta} = \frac{\beta + 1}{2\beta + 1} \qquad \text{(Eq g)}$$

After substitution of σ_m/σ_θ from Eq g, Eq 14 becomes:

$$\frac{2}{3} \int_0^{\bar{\varepsilon}_f} \frac{2\beta + 1}{\beta} d\bar{\varepsilon} = C_3 \qquad \text{(Eq h)}$$

Replacing $d\bar{\varepsilon}$ in Eq h with its value from Eq 4 gives:

$$\frac{4}{3\sqrt{3}} \int_0^{\varepsilon_{zf}} \left(2 + \frac{1}{\beta} \right) \sqrt{\beta^2 + \beta + 1} \, d\varepsilon_z = C_3 \qquad \text{(Eq 15)}$$

2.3.5 Oh et al. Criterion

In this fracture criterion, Oh et al. (Ref 7, 8) considered the ratio of the maximum tensile stress to the effective stress to be the important parameter in the case of ductile fracture. The criterion is expressed by:

$$\int_0^{\bar{\varepsilon}_f} \frac{\sigma_\theta}{\bar{\sigma}} d\bar{\varepsilon} = C_4 \qquad \text{(Eq 16)}$$

By substituting Eq 4 and 6 into Eq 16, the fracture criterion is reduced to:

$$\frac{2}{3} \int_0^{\varepsilon_{zf}} (2\beta + 1) \, d\varepsilon_z = C_4 \qquad \text{(Eq 17)}$$

2.3.6 Osakada and Mori Criterion

Osakada and Mori (Ref 9) developed a criterion that includes an explicit dependence on effective strain ($\bar{\varepsilon}$) in addition to mean stress (σ_m). It takes the form:

$$\int_0^{\bar{\varepsilon}_f} (B + \bar{\varepsilon} + D\sigma_m) \, d\bar{\varepsilon} = C_5 \qquad \text{(Eq 18)}$$

where B and D are material constants. The constant C_5 represents the critical effective strain accumulated over the strain path up to fracture.

By substituting σ_m from Eq 7, Eq 18 can be rewritten as:

$$\int_0^{\bar{\varepsilon}_f} B \, d\bar{\varepsilon} + \int_0^{\bar{\varepsilon}_f} \bar{\varepsilon} \, d\bar{\varepsilon} + \int_0^{\bar{\varepsilon}_f} D\sigma_m d\bar{\varepsilon} = C_5$$

$$B\bar{\varepsilon}_f + \frac{1}{2}\bar{\varepsilon}_f^2 + \frac{Dk}{\sqrt{3}} \left[\int_0^{\varepsilon_{zf}} \frac{\beta + 1}{\sqrt{\beta^2 + \beta + 1}} \left(\frac{2}{\sqrt{3}} \int_0^{\varepsilon_{zf}} \sqrt{\beta^2 + \beta + 1} \, d\varepsilon_z \right)^n d\varepsilon z \right] = C_5 \qquad \text{(Eq 19)}$$

where $\bar{\varepsilon}_f$ is given by Eq 5.

3. Results and Discussion

The six ductile fracture criteria outlined in section 2.3 have been reformulated such that each is expressed in terms of material-dependent quantities and constants, rather than in terms of stress and strain. Table 2 summarizes the criteria and quantities and constants that correspond to each criterion. Those quantities and constants include the flow-curve constants k and n; the

strain increment ratio, $\beta = d\varepsilon_\theta/d\varepsilon_z$; the axial fracture strain, ε_{zf}; and integration constants.

Principal strain space is traditionally used for the forming-limit curves to analyze failure in metalforming processes. The conventional way of representing strain in plane-strain loading ($\varepsilon_r = 0$) is in principal strain space, with ε_θ as the ordinate and ε_z as the abscissa. Nonlinear strain paths are considered to better represent actual applications.

The flow-curve constants k and n for the test materials are taken from Table 1. Experimentally determined strain-path curves, which give the complete plastic flow history of the material during the formation process, are used to find various values of the quantity β, which is generally a function of the axial strain, ε_z. It is known that the strain path for a given material under cold upsetting is a function of the equatorial strains on the surface, strain rate, temperature, friction, and specimen aspect ratio.

Now consider a strain path given by:

$$\varepsilon_\theta = a_1 \varepsilon_z^3 + a_2 \varepsilon_z^2 + a_3 \varepsilon_z \qquad \text{(Eq 20)}$$

Then,

$$\beta = \frac{d\varepsilon_\theta}{d\varepsilon_z} = 3a_1 \varepsilon_z^2 + 2a_2 \varepsilon_z + a_3$$

The constants a_1, a_2, and a_3 in Eq 20 are obtained using the experimental results obtained from the forming experiments conducted on a large number of specimens having various aspect ratios and under various friction conditions.

The constants in the fracture criteria (Eq 9, 11, 13, 15, 17, and 19) are evaluated by substituting the material constants k and n from Table 1 and the strain-path constants a_1, a_2, and a_3 and performing the integration from 0 to ε_{zf}. The resulting expressions give the fracture strains predicted by each criterion for a given material under the test conditions that are used to draw the forming limit diagrams.

The experimental strain-path curves used in this paper have been obtained from the literature for upsetting of aluminum and steel at room temperature (Ref 14-17). Typical experimental results for the axial and circumferential plastic principal strains at the equatorial free surface of upsetting aluminum and steel specimens of various aspect ratios, *H/D*, for lubricated and unlubricated platens are shown in Fig. 3 to 5. End points for all strain paths, which represent cracking or fracture, for a material give the forming limit diagram for this material.

Tables 3 to 5 give the axial fracture strain (ε_{zf}) and the strain increment ratio (β) for the test materials corresponding to specimen aspect ratio and lubrication condition. Tables 3 to 5 also summarize the constants that are evaluated upon integrating the criteria equations from 0 to ε_{zf}. The criteria equations in

Table 2 Summary of original and new forms of ductile fracture criteria and associated constants

Criterion	Original form of the criterion	New form of the criterion	Material-dependent quantities and constants
Oyane et al.	$\bar{\varepsilon}_f = -\frac{1}{A}\int_0^{\bar{\varepsilon}_f} \frac{\sigma_m}{\bar{\sigma}} d\bar{\varepsilon} + C$	$\bar{\varepsilon}_f = -\frac{2}{3A}\int_0^{\varepsilon_{zf}} (\beta + 1) d\varepsilon_z + C$ where $\bar{\varepsilon}_f = \frac{2}{\sqrt{3}}\int_0^{\varepsilon_{zf}} \sqrt{\beta^2 + \beta + 1}\, d\varepsilon_z$	$\beta, \varepsilon_{zf}, A, C$
Freudenthal	$\int_0^{\bar{\varepsilon}_f} \bar{\sigma}\, d\bar{\varepsilon} = C_1$	$\frac{k}{(n+1)}\left(\frac{2}{\sqrt{3}}\int_0^{\varepsilon_{zf}} \sqrt{\beta^2 + \beta + 1}\, d\varepsilon_z\right)^{n+1} = C_1$	$\beta, \varepsilon_{zf}, k, n, C_1$
Cockcroft and Latham	$\int_0^{\bar{\varepsilon}_f} \sigma_1\, d\bar{\varepsilon} = C_2$	$\frac{2k}{3}\int_0^{\varepsilon_{zf}} (2\beta + 1)(\bar{\varepsilon})^n\, d\varepsilon_z = C_2$ where $\bar{\varepsilon} = \frac{2}{\sqrt{3}}\int_0^{\varepsilon_{zf}} \sqrt{\beta^2 + \beta + 1}\, d\varepsilon_z$	$\beta, \varepsilon_{zf}, k, n, C_2$
Brozzo et al.	$\int_0^{\bar{\varepsilon}_f} \frac{2\sigma_1}{3(\sigma_1 - \sigma_m)} d\bar{\varepsilon} = C_3$	$\frac{4}{3\sqrt{3}}\int_0^{\varepsilon_{zf}} \frac{(2\beta + 1)}{\beta} \sqrt{\beta^2 + \beta + 1}\, d\varepsilon_z = C_3$	$\beta, \varepsilon_{zf}, C_2$
Oh et al.	$\int_0^{\bar{\varepsilon}_f} \frac{\sigma_1}{\bar{\sigma}} d\bar{\varepsilon} = C_4$	$\frac{2}{3}\int_0^{\varepsilon_{zf}} (2\beta + 1)\, d\varepsilon_z = C_4$	$\beta, \varepsilon_{zf}, C_3$
Osakada and Mori	$\int_0^{\bar{\varepsilon}_f} (B + \bar{\varepsilon} + D\sigma_m)\, d\bar{\varepsilon} = C_5$	$B\bar{\varepsilon}_f + \frac{1}{2}\bar{\varepsilon}_f^2 + \frac{Dk}{\sqrt{3}}\left[10\int_0^{\varepsilon_{zf}} \frac{(\beta + 1)}{\sqrt{\beta^2 + \beta + 1}} (\bar{\varepsilon})^n\, d\varepsilon_z\right] = C_5$ where $\bar{\varepsilon} = \frac{2}{\sqrt{3}}\int_0^{\varepsilon_{zf}} \sqrt{\beta^2 + \beta + 1}\, d\varepsilon_z$	$\beta, \varepsilon_{zf}, k, n, B, D, C_5$

their new forms are then plotted graphically in Fig. 6 to 8, which show "theoretically" predicted forming limit diagrams. For the purpose of comparison, the theoretically predicted and the experimentally obtained forming limit diagrams are superimposed in Fig. 9 to 11. This comparison is also summarized in Tables 6 to 8. Reasonable agreement exists between theoretical and experimental predictions of ductile fracture for most of the criteria assessed in this study.

Table 9 summarizes the percentage difference between experimental and criteria predictions of fracture strains for the three materials considered. In addition, the relationships between the experimental and criteria predictions are shown graphically in Fig. 12 to 17. It can be seen that five of the fracture criteria tested in this study are quite successful in predicting the fracture strain in upsetting processes to very limited percentage differences. The most successful criteria are those of Oyane et al. (Ref 2, 3) and Oh et al. (Ref 7, 8), where the average percentage differences in their predictions of fracture strain are approximately 2.4 and 3.0%, respectively. Average percentage differences in the predictions made

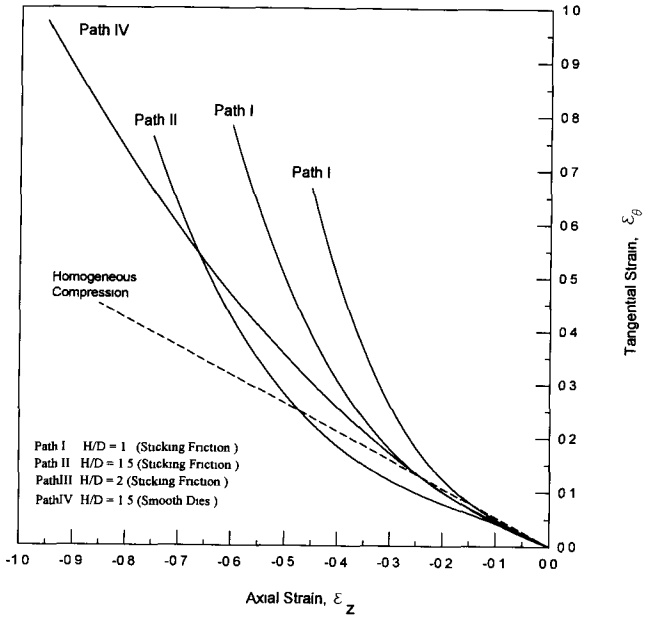

Fig. 3 Typical experimental strain paths for low-alloy steel. Source: Ref 14

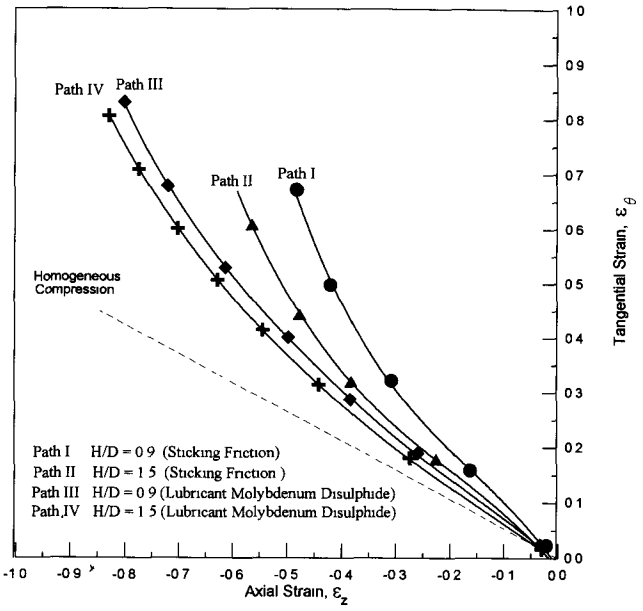

Fig. 4 Typical experimental strain paths for spheroidized steel. Source: Ref 15

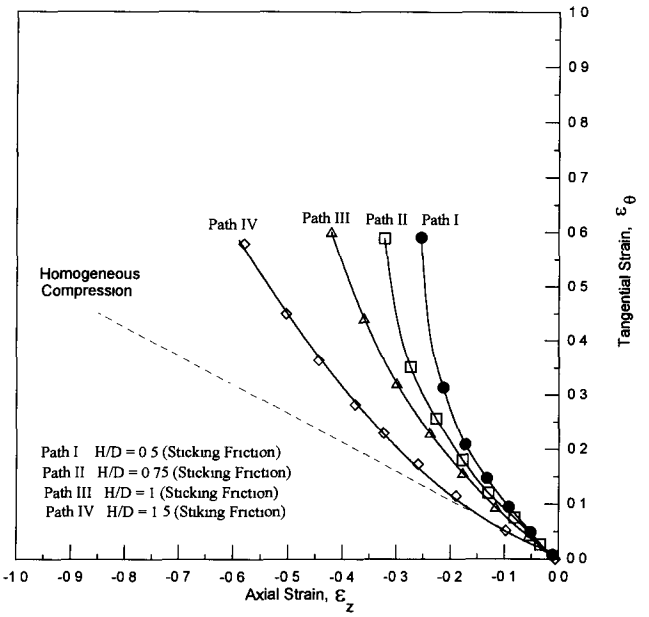

Fig. 5 Typical experimental strain paths for commercially pure aluminum. Source: Ref 16, 17

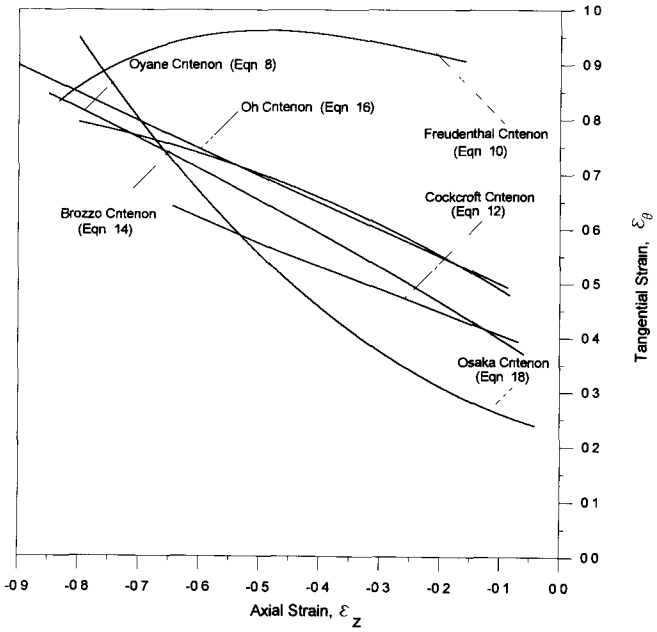

Fig. 6 Graphical plots of the fracture criteria indicating predictions of fracture strains for low-alloy steel

by the criteria of Brozzo et al. (Ref 6), Cockcroft and Latham (Ref 5), and Freudenthal (Ref 4) are shown to be 4.2, 5.5, and 6.8%, respectively. Large deviations, up to –31%, are found in the predictions made by the Osakada and Mori (Ref 9) criterion.

It is also apparent that the highly successful criteria are those which include the effect of hydrostatic stress—a critical factor in the mechanism of void initiation, growth, and coalescence. Tensile hydrostatic stress enhances the void initiation, growth, and coalescence process, leading to lower fracture strains. Compressive hydrostatic stress, on the other hand, leads to higher fracture strains.

The Cockcroft and Latham criterion predicts lower values of fracture strains for upsetting processes. This criterion considers the effects of the maximum principal tensile stress over the plastic strain path to failure and includes an implicit dependence on hydrostatic stress. The modifications made by Brozzo et al. and Oh et al. with the explicit dependence on hydrostatic stress greatly improved fracture strain predictions.

Table 3 Material-dependent quantities (β and ε_{zf}) and calculated constants in various ductile fracture criteria for pure aluminum

Strain path	Strain increment ratio, $\beta = d\varepsilon_\theta/d\varepsilon_z$	Axial fracture strain, ε_{zf}	Ductile fracture criterion					
			Oyane et al.	Freudenthal	Cockcroft and Latham	Brozzo et al.	Oh et al.	Osakada and Mori
I	$-255.045\varepsilon_z^2 - 48.2\varepsilon_z - 2.93$	–0.253						
II	$-95.1\varepsilon_z^2 - 21.6\varepsilon_z - 2.0$	–0.321	A = 0.3273					$C_5 = 0.019$
III	$-15.9\varepsilon_z^2 - 2.0\varepsilon_z - 0.91$	–0.420	C = 0.98151	$C_1 = 144$	$C_2 = 59.084$	$C_3 = -0.6153$	$C_4 = 0.6031$	B = 0.323
IV	$-3.9\varepsilon_z^2 - 0.1\varepsilon_z - 0.6$	–0.589						D = 0.0017

Table 4 Material-dependent quantities (β and ε_{zf}) and calculated constants in various ductile fracture criteria for low-alloy steel

Strain path	Strain increment ratio, $\beta = d\varepsilon_\theta/d\varepsilon_z$	Axial fracture strain, ε_{zf}	Ductile fracture criterion					
			Oyane et al.	Freudenthal	Cockcroft and Latham	Brozzo et al.	Oh et al.	Osakada and Mori
I	$-19.2\varepsilon_z^2 - 1.4\varepsilon_z - 0.5$	–0.45						
II	$-10.2\varepsilon_z^2 - 1.4\varepsilon_z - 0.5$	–0.64	A = –0.522					$C_5 = -0.12$
III	$-6.75\varepsilon_z^2 - 2.0\varepsilon_z - 0.5$	–0.75	C = –0.64	$C_1 = -82$	$C_2 = -75$	$C_3 = 0.472$	$C_4 = 0.46$	B = 0.51
IV	$1.4\varepsilon_z - 0.36$	–0.95						D = –0.001

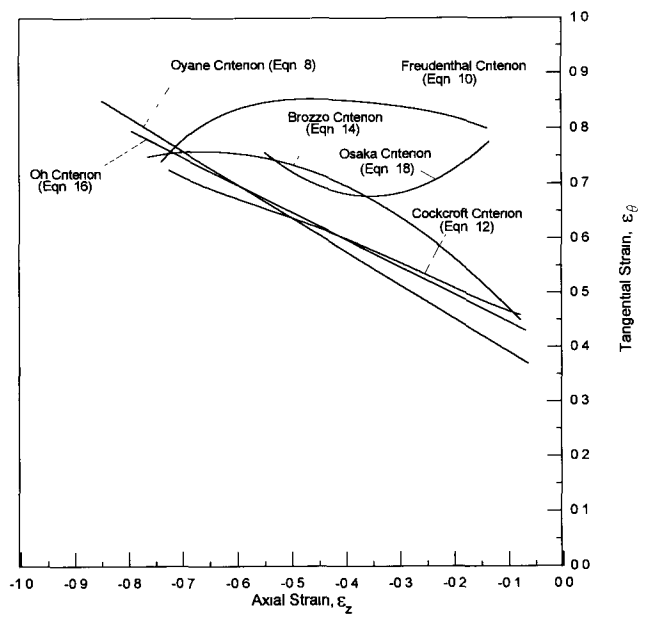

Fig. 7 Graphical plots of the fracture criteria indicating predictions of fracture strains for spheroidized steel

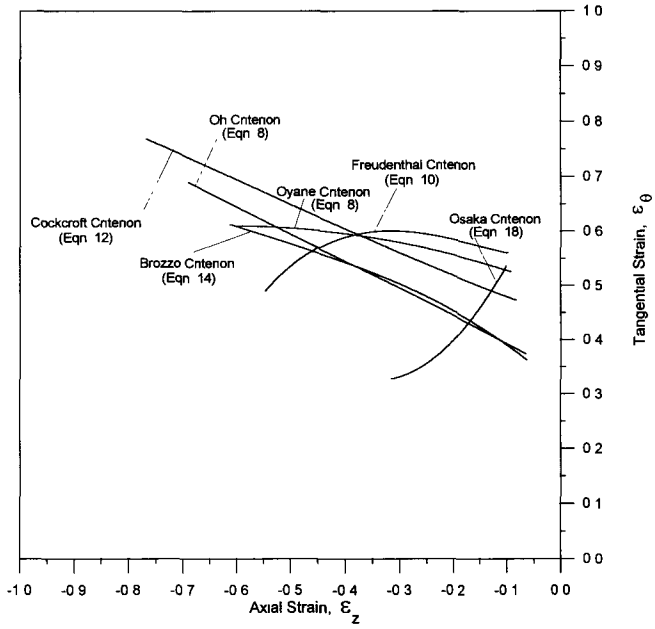

Fig. 8 Graphical plots of the fracture criteria indicating predictions of fracture strains for commercially pure aluminum

Highly accurate predictions also result from the Oyane et al. criterion, which is based on the void growth theory. This type of criterion is based on the presence of voids in the material before subjection to load. Thus, the void initiation phase is bypassed, with voids present very early in the deformation sequence. In addition, the fracture propagation rate is considered to be low so that the void growth phase is dominant. Predictions made by such criteria are accurate within about –7.5 to +3.5%. It is worth noting that the Oyane criterion includes explicit dependence on hydrostatic stress.

Table 5 Material-dependent quantities (β and ε_{zf}) and calculated constants in various ductile fracture criteria for spheroidized steel

Strain path	Strain increment ratio, $\beta = d\varepsilon_\theta/d\varepsilon_z$	Axial fracture strain, ε_{zf}	Ductile fracture criterion					
			Oyane et al.	Freudenthal	Cockcroft and Latham	Brozzo et al.	Oh et al.	Osakada and Mori
I	$-14.7\varepsilon_z^2 - 4.0\varepsilon_z - 1.17$	–0.48						
II	$-8.91\varepsilon_z^2 - 3.0\varepsilon_z - 1.0$	–0.60	A = –0.264					$C_5 = 0.129$
III	$-2.49\varepsilon_z^2 - 0.7\varepsilon_z - 0.77$	–0.80	C = –0.85	$C_1 = 345$	$C_2 = -195$	$C_3 = -0.59$	$C_4 = 0.53$	B = 0.4
IV	$1.90\varepsilon_z^2 - 0.392\varepsilon_z - 0.36$	–0.83						D = –0.004

Table 6 Experimental and predicted axial fracture strains for low-alloy steels

Strain path	Axial compressive fracture strain, ε_{zf}						
	Experimental	Predicted for various fracture criteria					
		Oyane et al.	Oh et al.	Brozzo et al.	Cockcroft and Latham	Osakada and Mori	Freudenthal
I	0.45	0.436	0.453	0.455	0.413	0.348	0.527
II	0.60	0.57	0.586	0.584	0.535	0.535	0.649
III	0.75	0.763	0.774	0.757	0.718	0.800	0.78
IV	0.95	0.879	0.905	0.846	0.787	...	0.852

Table 7 Experimental and predicted axial fracture strains for spheroidized steel

Strain path	Axial compressive fracture strain, ε_{zf}						
	Experimental	Predicted for various fracture criteria					
		Oyane et al.	Oh et al.	Brozzo et al.	Çockcroft and Latham	Osakada and Mori	Freudenthal
I	0.480	0.470	0.474	0.507	0.477	0.500	0.531
II	0.600	0.606	0.606	0.629	0.600	0.672	0.649
III	0.800	0.801	0.785	0.762	0.76	...	0.751
IV	0.83	0.861	0.844	0.795	0.825	...	0.766

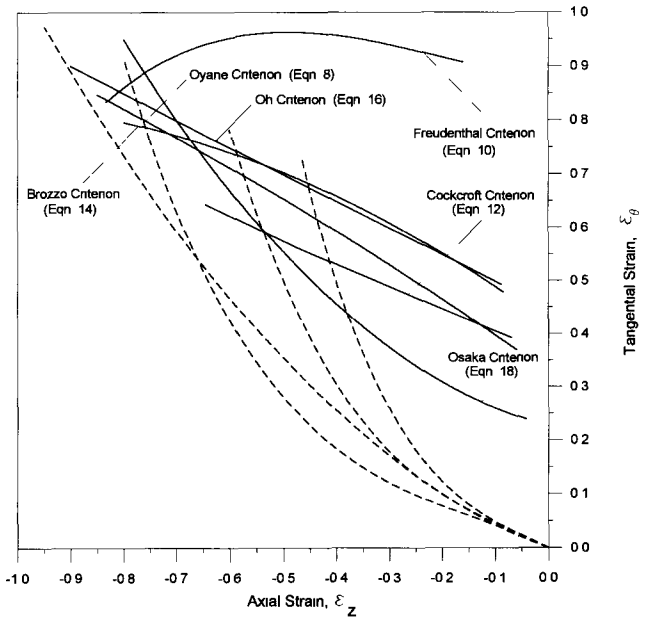

Fig. 9 Criteria predictions and experimental fracture strains for low-alloy steel

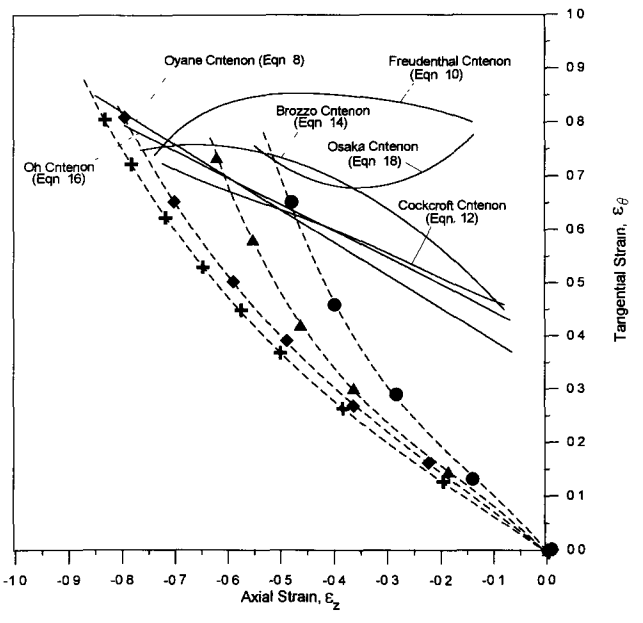

Fig. 10 Criteria predictions and experimental fracture strains for spheroidized steel

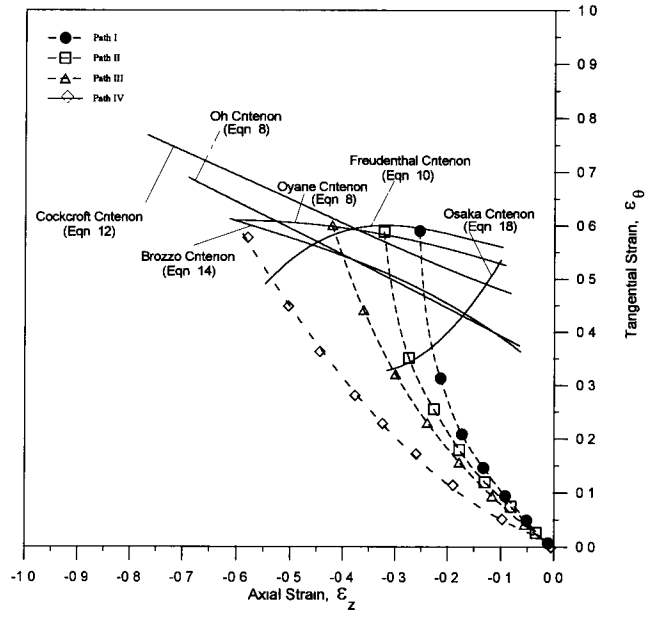

Fig. 11 Criteria predictions and experimental fracture strains for commercially pure aluminum

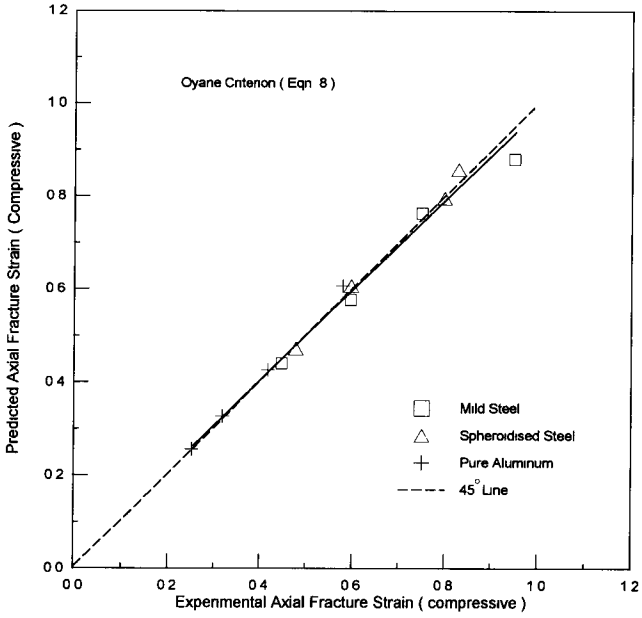

Fig. 12 Experimental fracture strains versus predictions obtained using the Oyane et al. criterion

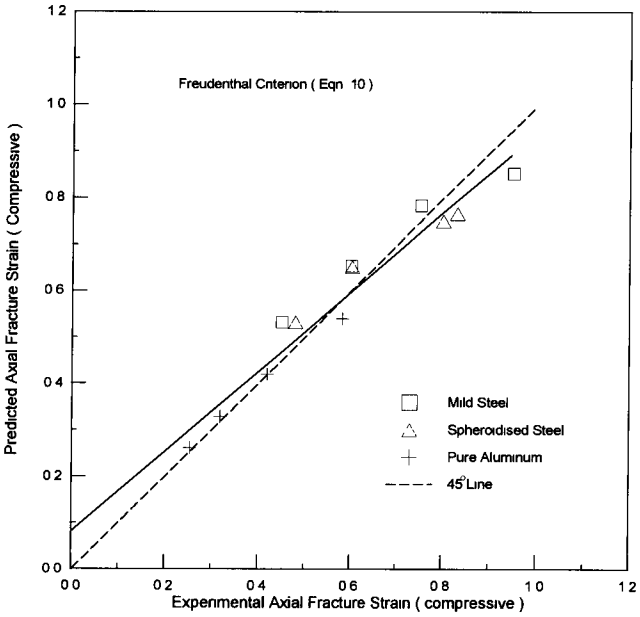

Fig. 13 Experimental fracture strains versus predictions obtained using the Freudenthal criterion

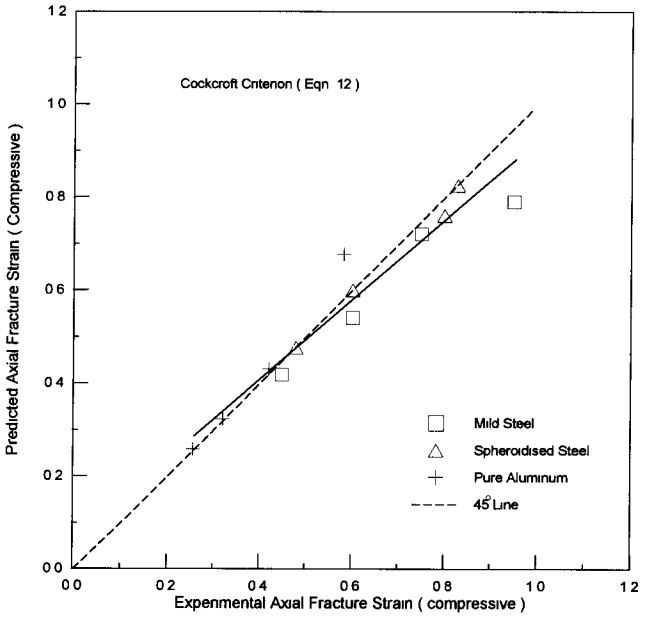

Fig. 14 Experimental fracture strains versus predictions obtained using the Cockcroft and Latham criterion

Table 8 Experimental and predicted axial fracture strains for pure aluminum

	Axial compressive fracture strain, ε_{zf}						
		Predicted for various fracture criteria					
Strain path	Experimental	Oyane et al.	Oh et al.	Brozzo et al.	Cockcroft and Latham	Osakada and Mori	Freudenthal
I	0.256	0.253	0.246	0.247	0.253	0.232	0.256
II	0.321	0.321	0.311	0.311	0.319	0.272	0.321
III	0.420	0.420	0.402	0.402	0.426	0.305	0.415
IV	0.580	0.600	0.630	0.603	0.675	0.400	0.534

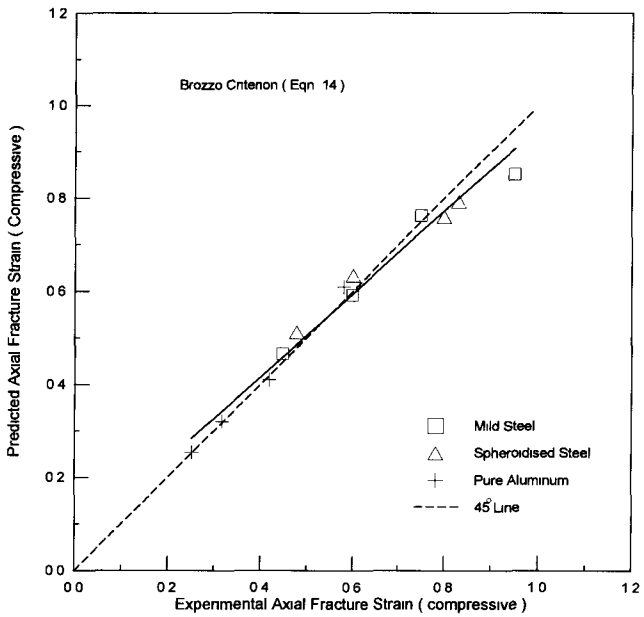

Fig. 15 Experimental fracture strains versus predictions obtained using the Brozzo et al. criterion

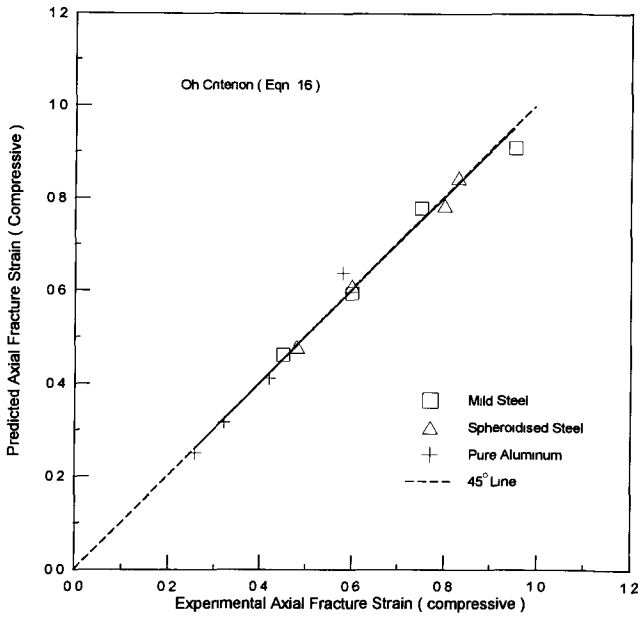

Fig. 16 Experimental fracture strains versus predictions obtained using the Oh et al. criterion

Table 9 Summary of fracture strain predictions

Strain path	Percentage difference					
	Oyane et al.	Freudenthal	Cockcroft and Latham	Brozzo et al.	Oh et al.	Osakada and Mori
Low-alloy steel						
I	–3.11	+17.11	–8.22	+1.11	–0.67	–22.67
II	–5.00	+8.17	–10.83	–2.67	– 2.33	–10.83
III	+1.73	+4.00	–4.27	+0.93	+3.20	+6.67
IV	–7.47	–10.32	–17.16	–10.95	–4.74	...
Spheroidized steel						
I	–2.10	+10.63	–0.63	+5.63	–1.25	–4.17
II	+1.00	+8.17	0	+4.84	1.00	+12.00
III	+0.13	–6.13	–4.75	–4.75	–1.88	...
IV	+3.74	–7.71	–0.60	–4.22	+1.69	...
Aluminum						
I	–1.17	0	–1.17	–3.52	–3.90	–9.38
II	0	0	–0.62	–3.12	–3.12	–15.26
III	0	–1.19	+1.43	–4.29	–4.29	–27.38
IV	+3.45	–7.93	+16.38	+3.97	+8.62	–31.03

The fracture initiation predictions from the Osakada and Mori criterion, which also contains an explicit dependence on hydrostatic stress, have not been very successful. The terms in this criterion require closer investigation in order to make it more suitable for predicting fracture in upsetting processes.

All of the tested criteria exhibit the largest percentage differences between experimental and theoretical predictions for strain path IV for aluminum and low-alloy steel. Path IV is the closest to homogeneous compression; that is, no friction exists between specimen and platens. All criteria should contain an additional "constraining" term to account for the lubrication condition, which has a direct relation to the state of stress on the equatorial surface of the specimen. Lower predictions were made by most of the criteria for low-alloy steel, whereas higher predictions were made for the commercially pure aluminum.

4. Conclusions

Despite the differences found between the experimental and criteria predictions of fracture strains during upsetting processes, the empirical and semiempirical ductile fracture criteria studied here are successful, to a certain degree, in predicting fracture strain during upsetting processes. The reformulations of the original criteria that were suggested by Kivivuori et al. (Ref 14) and used in this study improve the useability of the criteria. The criteria are expressed in terms of material-dependent

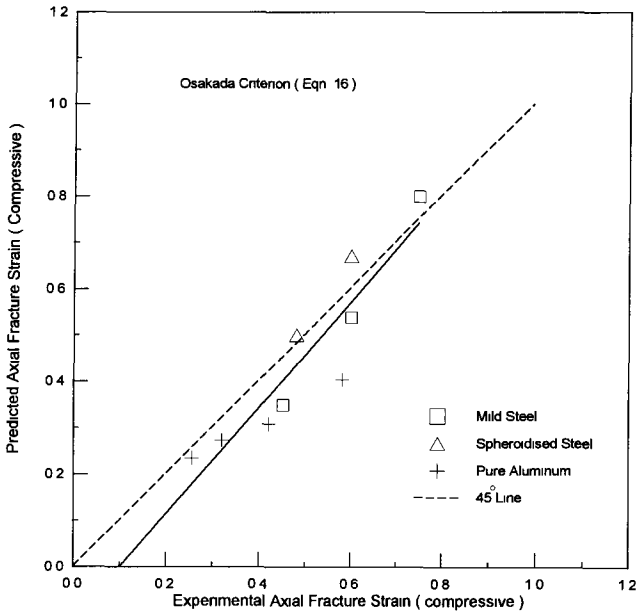

Fig. 17 Experimental fracture strains versus predictions obtained using the Osakada and Mori criterion

quantities and integration constants instead of stresses and strain. However, determination of the constants in the new forms of the criteria is still rather laborious and, in some cases, cumbersome.

References

1. S.E. Clift and P. Hartley, Fracture Prediction in Plastics Deformation Processes, *Int. J. Mech. Sci.*, Vol 32 (No. 1), 1990
2. M. Oyane, Criteria of Ductile Fracture Strain, *Bull. Jpn. Soc. Mech. Eng.*, Vol 15, 1972, p 1507-1513
3. M. Oyane, T. Sato, K. Okimoto, and S. Shima, Criteria for Ductile Fracture and Their Applications, *J. Mech. Work. Technol.*, No. 4, 1980, p 65-81
4. A.M. Freudenthal, *The Inelastic Behaviour of Solids*, John Wiley & Sons, 1950
5. M.G. Cockcroft and D.J. Latham, Ductility and the Workability of Metals, *J. Inst. Met.*, Vol 96, 1968, p 33-39
6. P. Brozzo, B. Deluca, and R. Rendina, A New Method for the Prediction of Formability Limits in Metal Sheets, *Proc. 7th Biennial Conf. of the Int. Deep Drawing Research Group*, 1972
7. S.I. Oh and S. Kobayashi, "Theories of Flow and Fracture in Metal-Forming Processes, Part 2: A Theory on Ductile Fracture in Metal-Working Processes," Technical Report, Air Force Material Laboratory, OH, AFML-TR-76-61, 1976
8. S.I. Oh, C.C. Chen, and S. Kobayshi, Ductile Fracture in Axisymmetric Extrusion and Drawing, Part 2: Workability in Extrusion and Drawing, *J. Eng. Ind. (Trans. ASME)*, Vol 101, 1979, p 36-48
9. K. Osakada and K. Mori, Prediction of Ductile Fracture in Cold Forging, *Ann. CIRP*, Vol 27, 1978, p 135-139
10. P. Hartley, S.E. Clift, J. Salimi-Namin, C.E.N. Sturgess, and I. Pillinger, The Prediction of Ductile Fracture Initiation in Metal-forming Using a Finite Element Method and Various Fracture Criteria, *Res. Mech.*, Vol 28, 1989, p 269-293
11. I. Pillinger, "The Prediction of Metal Flow and Properties in Three-Dimensional Forging Using the Finite Element Method," Ph.D. thesis, University of Birmingham, 1984
12. N.L. Dung, Identification of Defect Locations in Metal-Forming Using a Personal-Computer-Oriented Finite Element Method, *Modelling of Metal Forming Processes*, J.L Chnot and E. Orate, Ed., Klumer Academic, The Netherlands, 1988, p 245-252
13. G. LeRoy J.D. Embury, G. Edward, and M.F. Ashby, A Model of Ductile Fracture Based on the Nucleation and Growth of Voids, *Acta Metall.*, Vol 29, 1981, p 1509-1522
14. S. Kivivuori, I. Lahti, and V. Ollilainen, A Computational Method to Estimate the Formability of Cold Forming Steels, *Computational Methods for Predicting Material Processing Defects*, M. Predeleana, Ed., Elsevier Science, Amsterdam, 1987, p 193-202
15. S.S. Hecker, *Formability: Analysis, Modelling and Experimentation*, TMS-AIME, 1977, p 150-182
16. P.F. Thomason, *Ductile Fracture of Metals*, Pergamon Press, 1990
17. P.F. Thomason, The Use of Pure Aluminum as an Analogue for the History of Plastic Flow in Studies of Ductile Fracture Criteria in Steel Compression Specimens, *Int. J. Mech. Sci.*, Vol 10, 1968, p 501-518